A Model for Gas Transport in Microfractures of Shale and Tight Gas Reservoirs

Keliu Wu
Chemical and Petroleum Engineering, University of Calgary, Calgary, Alberta T2N1N4, Canada

Key Laboratory for Petroleum Engineering of the Ministry of Education, China University of Petroleum, Beijing 102249, China

Xiangfang Li
Key Laboratory for Petroleum Engineering of the Ministry of Education, China University of Petroleum, Beijing 102249, China

Chenchen Wang and Zhangxin Chen
Chemical and Petroleum Engineering, University of Calgary, Calgary, Alberta T2N1N4, Canada

Wei Yu
Petroleum and Geosystems Engineering, The University of Texas at Austin, Austin, Texas 78712, United States

DOI 10.1002/aic.14791
Published online March 27, 2015 in Wiley Online Library (wileyonlinelibrary.com)

A model for gas transport in microfractures of shale and tight gas reservoirs is established. Slip flow and Knudsen diffusion are coupled together to describe general gas transport mechanisms, which include continuous flow, slip flow, transitional flow, and Knudsen diffusion. The ratios of the intermolecular collision frequency and the molecule-wall collision frequency to the total collision frequency are defined as the weight coefficients of slip flow and Knudsen diffusion, respectively. The model is validated by molecular simulation results. The results show that: (1) the model can reasonably describe the process of the mass transform of different gas transport mechanisms; (2) fracture geometry significantly impacts gas transport. Under the same fracture aperture, the higher the aspect ratio is, the stronger the gas transport capacity, and this phenomenon is more pronounced in the cases with higher gas pressure and larger fracture aperture. © 2015 American Institute of Chemical Engineers *AIChE J*, 61: 2079–2088, 2015
Keywords: shale gas reservoirs, tight gas reservoirs, micro fracture, slip flow, knudsen diffusion

Introduction

In the process of diagenesis and hydrocarbon evolution in shale and tight sandstone reservoirs, pores and microfractures are generated due to stress variation and hydrothermal fluids produced.[1,2] Planar and regular microfractures with apertures of 0.06–3.3 μm are created in weak planes of tight sandstone reservoirs (Figures 1a, b),[2,3] while regular and irregular microfractures are formed in weak planes or organic matter edges of shale reservoirs (Figure 1c).[4] The length and aperture of microfractures in shale and tight sandstone reservoirs usually distribute in the nano-microscale with different orientations (Figure 2).[2,3] The microfractures with complex geometry are generally simplified to parallel planar fractures with smooth surfaces to approximately describe gas flow in shale and tight gas reservoirs.[5–8]

Gas transport mechanisms in microfractures

Pressure varies in microfractures with the aperture of nano-microscale distribution[2–4,9–11] during the development of gas reservoirs.[12,13] The typical value of Knudsen number (Kn) ranges from 0.00005 to 2.[14] Knudsen number refers to the ratio of gas mean-free-path to microfracture aperture. The gas transport process is governed by different mechanisms, including continuum flow, slip flow, and transition flow, which can be determined based on the different range of Knudsen number, as illustrated in Table 1.[5,7] Different gas transport mechanisms should be characterized with the corresponding constitutive equations.[15,16] An accurate description of each mechanism plays an important role in the dynamic production analysis in shale and tight sandstone gas reservoirs.[17]

Microfracture shape and size are the key parameters affecting or determining the gas transport mechanisms and apparent permeability; especially, the microfracture aperture has a significant impact on the economic development of shale and tight sandstone gas reservoirs.[2,18–27] Gas transport constitutive equations should consider the effects of the microfracture shape and size.[5,7,28] Smolouchowski[29] proposed a correction factor for the influence of a microfracture rectangular section on gas Knudsen diffusion; Kennard[30] also derived a similar correction factor, which was adopted by Eldridge and Brown[31]; Matson and Quinn[32] found that

Correspondence concerning this article should be addressed to K. Wu at wukeliu19850109@163.com.

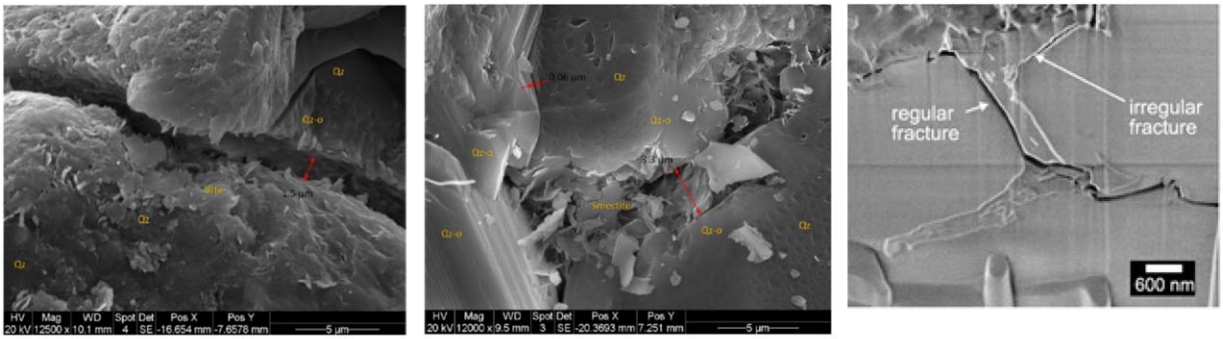

(a) Planar micro fractures in tight Nikanassin formation in Canada [2, 3]

(b) Regular micro fractures in tight Nikanassin formation in Canada [2, 3]

(c) Regular or irregular micro fractures in Woodford shale in USA[4]

Figure 1. Microfractures in shale and tight gas reservoirs.

(a) Planar microfractures in tight Nikanassin formation in Canada,[2,3] (b) Regular microfractures in tight Nikanassin formation in Canada,[2,3] and (c) Regular or irregular microfractures in Woodford shale in the United States.[4] [Color figure can be viewed in the online issue, which is available at wileyonlinelibrary.com.]

the influence of section shape on gas Knudsen diffusion cannot be ignored, particularly a microfracture section has a high aspect ratio (a ratio of microfracture width to aperture); White indicated that the section shape has a significant influence on gas continuous flow and the corresponding correction factor was introduced.[33] However, there have been very few studies that have investigated the influences of both microfracture sizes and section shape at the same time on the different gas transport mechanisms.

Mathematical models for gas transport in microfractures

Due to high gas compressibility and stress-dependent permeability, the gas transport mechanism is quite different from that of liquid in microfractures.[34] Generally, the gas transport in microfractures may be described by molecular and continuity models.[7]

A molecular model, which is also referred to as molecular simulation, mainly includes a direct-simulation Monte Carlo method,[35] a molecular dynamics simulation method[36] and a lattice Boltzmann method.[37] The molecular simulation considers the attributes of gas molecules with high accuracy.[38,39] However, it consumes huge computational resources and time, which could not be suitable for gas transport simulation in microfractures of shale and tight sandstone reservoirs.[38–43]

A continuity model, which is known as Poiseuille's equation, can be used to describe the variation of gas macroscopic properties with space and time and is widely applied for the gas transport simulation.[44] However, under conditions of low pressure and small microfracture aperture, the gas molecules slip on the walls and the continuity condition is not valid, resulting in the continuity model that could not accurately describe the gas transport.[45]

A slip model was derived with a modification of a nonslip boundary condition based on the continuity model,[4] which is widely used to calculate the shale gas transport.[5,46–51] The slip model mainly includes a first-order slip model,[52] a second-order slip model,[53] and a Beskok–Karniadakis model.[54] Application results show that the first-order slip model underestimates the gas transport rate, and the deviation increases with an increasing of the Knudsen number;[16] the second-order slip model overestimates the gas transport rate;[16] the Beskok and Karniadakis model introduces a rarefaction coefficient to improve the accuracy of these two models; however, the deviation of estimating gas fluxes on the walls is still high.[16] Thompson and Owens[19] indicated that when the Knudsen number is higher, the slip model cannot degrade into a Knudsen diffusion equation and cannot be used to describe the Knudsen diffusion. Hence, the current slip models cannot accurately describe the gas transport process with different Knudsen numbers.

Due to the limitations of the continuity model and the slip model, many authors have tried to build a unified gas

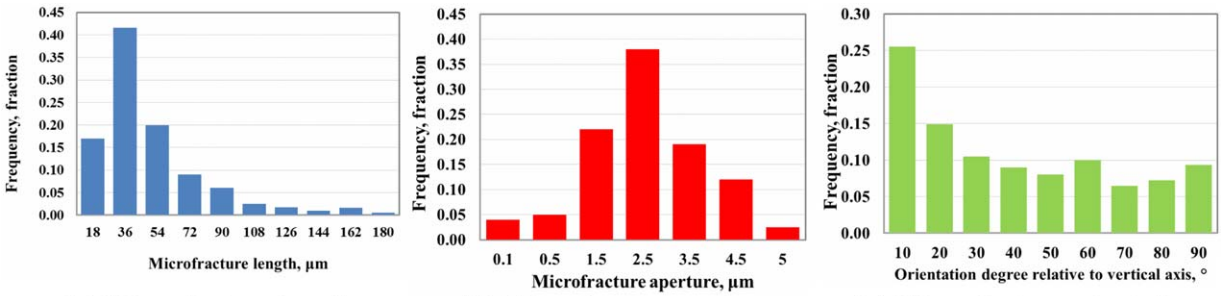

(a) Micro fracture length

(b) Micro fracture aperture

(c) Micro fracture orientation

Figure 2. Typical microfracture distribution extracted from high resolution thin-section image processing in tight gas Nikanassin formation in Canada.[2,3]

(a) Microfracture length, (b) Microfracture aperture, and (c) Microfracture orientation. [Color figure can be viewed in the online issue, which is available at wileyonlinelibrary.com.]

Table 1. Different Flow Regimes as a Function of the Knudsen Number[5]

Knudsen number (*Kn*)		
Lower limit	Upper limit	Gas transport mechanism
0	10^{-3}	Continuum or Darcy flow (no-slip)
10^{-3}	10^{-2}	Slip flow
10^{-2}	10^{-1}	
10^{-1}	10^{0}	Transition flow
10^{0}	10^{1}	

transport model which could describe several transport mechanisms with the combination of models for each mechanism, as summarized in Table 2.

So far, a lot of gas transport models were proposed. However, some models contain unreasonable weight coefficients, while the other models contain empirical coefficients or are only suitable for gas transport with a circular section. Hence, a unified model that covers a fuller spectrum of transport mechanisms is still required for microfractures with a rectangular section. Such a model is of practical significance to the development of shale and tight sandstone gas reservoirs.

Slip flow and Knudsen diffusion are two different gas transport mechanisms. The slip flow occurs when the intermolecular collision dominates, and the Knudsen diffusion takes place when the wall-molecule collision dominates.[15,19] Based on the slip flow and Knudsen diffusion, a gas transport model in microfractures of shale and tight sandstone reservoirs is proposed by coupling these two transport mechanisms together using the weighted coefficients based on the ratios of intermolecular collision frequency and wall-molecule collision frequency to the total collision frequency. As shown in the remaining of this article, this model can account for continuum flow, slip flow, transition flow, and Knudsen diffusion. The influences of microfracture section shape, sizes, and pressure on the gas transport are examined based on this model.

Four parts are included in this article: first, different gas transport mechanisms are elaborated and coupled to build the gas transport model in microfractures of shale and tight sandstone reservoirs; second, the model is validated by published molecular simulation results; the third part is sensitivity analysis analyzing the impacts of microfracture section shape, sizes, and gas pressure on the gas transport, and the contributions of slip flow and Knudsen diffusion to the gas transport are also discussed under different production stages; the last part is a conclusion.

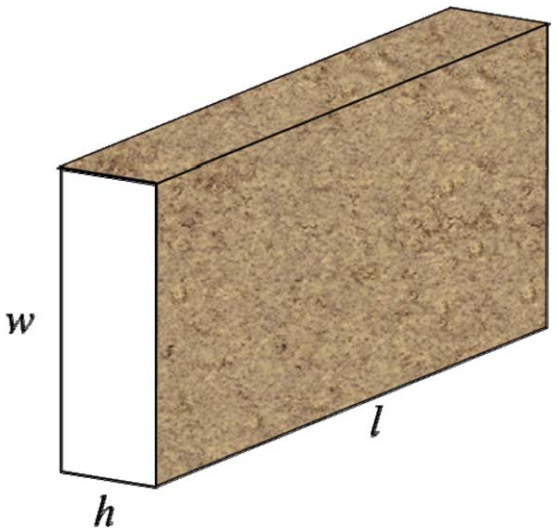

Figure 3. Scenario of simplified microfracture model.

[Color figure can be viewed in the online issue, which is available at wileyonlinelibrary.com.]

Model

A microfracture in shale and tight gas reservoirs can be simplified to a plane with rectangular section,[6] as shown in Figure 3. The section geometric parameter of a microfracture can be represented as follows

Table 2. Comparison and Evaluation of Different Gas Transport Models

Model	Description	Limitation
Adzumi[55–57]	Combination of continuum flow and Knudsen diffusion with contribution weight	Contribution weight factors are not given
Brown et al.[58]	Combination of continuum flow and slip flow with linear additivity	Only for circular section
Scott and Dullien[59]	Combination of slip flow and Knudsen diffusion with contribution weight	Only for circular section
Browne and John[15]	Combination of slip flow and Knudsen diffusion with contribution weight	Only for radial flow
Thompson and Owens[19]	Combination of slip flow and Knudsen diffusion with contribution weight	Only for circular section
Ertekin et al.[60]	Combination of continuum flow and Fick diffusion with constant contribution weight	Contribution weight factors are constant
Liu et al.[61]	Combination of continuum flow and Knudsen diffusion with flow section as the contribution weight	Only for circular section
Javadpour[46]	Combination of slip flow and Knudsen diffusion with linear additivity	Contribution weight is "1"
Li et al.[62]	Combination of continuum flow and Knudsen diffusion with contribution weight	Only for circular section
Prince and Javadpour[50]	Similar with Javadpour,[46] real gas is considered	Contribution weight is "1"
Darabi et al.[51]	Similar with Javadpour,[46] the influence of wall roughness on Knudsen diffusion is considered.	Contribution weight is "1"
Singh and Javadpour[5]	Combination of convection and Fick diffusion with linear additivity, the influence of section shape is considered	Contribution weight is "1"
Mohammad et al.[7]	Combination of continuum flow and Knudsen diffusion with contribution weight, only the influence of section shape on Knudsen diffusion is considered	Contribution weight is determined by experimental data

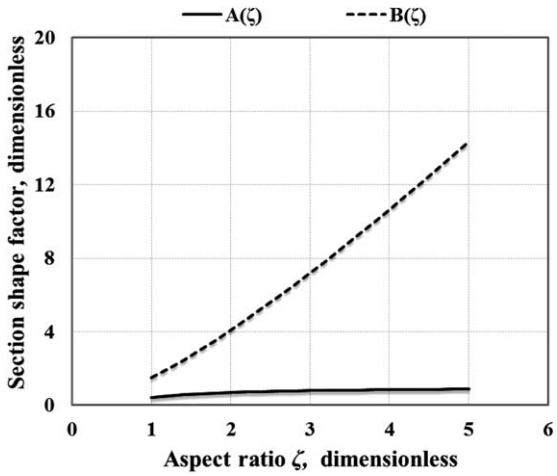

Figure 4. The curves for section shape factor with aspect ratio.

$$\zeta = \frac{w}{h} \tag{1}$$

where ζ is the aspect ratio of the microfracture, dimensionless; w is the width of the microfracture, m; h is the aperture of the microfracture, m.

The Knudsen number (Kn) of a microfracture is expressed below[19,28]

$$Kn = \frac{\lambda}{h} \tag{2}$$

where λ is the gas mean free path, m. The Knudsen number is a characterization parameter of a rarefaction effect, which can be used to determine the different gas transport mechanisms.[7]

The gas mean free path can be expressed as[63]

$$\lambda = \frac{\mu}{p}\sqrt{\frac{\pi RT}{2M}} \tag{3}$$

where μ is the gas viscosity, $P_a \cdot s$; R is the universal gas constant, J/mol/K; T is formation temperature, K; p is the average pressure between inlet and outlet of a single microfracture, Pa; M is gas molar mass, kg/mol.

Continuum flow

When $K_n < 10^{-3}$, the intermolecular collisions dominate and gas flow is continuum flow, which satisfies the continuity condition and can be expressed with the Hagen–Poiseuille equation[5,64]

$$J_v = -\frac{\phi}{\tau}\frac{wh^3}{12\mu}\frac{pM}{RT}\frac{dp}{dl} \tag{4}$$

where J_v is the mass flux of gas continuum flow in microfractures, kg/s; ϕ is the porosity of microfractures, fraction; τ is the tortuosity of microfractures, dimensionless; l is the length of the microfracture, m.

Equation 4 considers the influence of the microfracture porosity and tortuosity on gas transport, illustrating that the continuum flux is inversely proportional to gas viscosity and proportional to gas pressure and the gas transport flux will be very low under low pressure.[65]

Considering the influences of the section geometry and size, the gas continuum flow in microfractures can be expressed as[28]

$$J_v = -A(\zeta)\frac{\phi}{\tau}\frac{wh^3}{12\mu}\frac{pM}{RT}\frac{dp}{dl} \tag{5}$$

where

$$A(\zeta) = 1 - \frac{192}{\zeta\pi^5}\sum_{i=1,3,5,\ldots}^{\infty}\frac{\tanh(i\pi\zeta/2)}{i^5} \tag{6}$$

where $A(\zeta)$ is the section shape factor of microfractures with the continuum flow, dimensionless, which is not influenced by the variation of Kn, as shown in Figure 4.

Slip flow

When $10^{-3} < Kn < 10^{-1}$, both the intermolecular and wall-molecule collisions are comparable and gas molecules slip on the wall. With a modification of the slip boundary condition, the gas slip flow can be expressed as[28]

$$J_{vs} = -A(\zeta)\frac{\phi}{\tau}\frac{wh^3}{12\mu}\frac{pM}{RT}(1+\alpha Kn)\left(1+\frac{6Kn}{1-bKn}\right)\frac{dp}{dl} \tag{7}$$

where J_{vs} is the mass flux of gas slip flow in microfractures, kg/s; b is a gas slip constant, dimensionless. If the boundary is a first-order slip boundary, $b = 0$; if the boundary is a second-order slip boundary, $b = -1$; α is a rarefaction coefficient, dimensionless.

Molecular simulation results show that the gas slip constant $b = -1$ is more reasonable within the different Knudsen numbers. The rarefaction coefficient is defined to describe the physical phenomenon that the gas viscosity decreases with an increase in the Knudsen number. It equals to 0 during the continuum flow region and increases to a constant value during molecular flow (this value is a specific constant for a specific microfracture and gas system), and it depends on the section shape and gas pressure of microfractures.[7] A lot of experimental or molecular simulation data are needed to determine the rarefaction coefficients under different Knudsen numbers. According to molecular simulation results, the relationships of the rarefaction coefficient and Knudsen number with different aspect ratios in microfractures are shown in Figure 5.[28]

Equation 7 also shows that the slip effect is obvious with an increase in the Knudsen number, and the gas transport

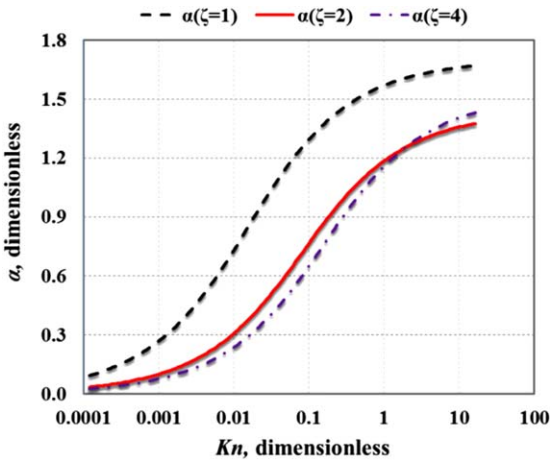

Figure 5. The curves for $\alpha \sim Kn$ with different aspect ratios.[28]

[Color figure can be viewed in the online issue, which is available at wileyonlinelibrary.com.]

Table 3. Summary of Modeling Parameters Used in the Calculations

Parameters	Symbol (Unit)	Value
Microfracture porosity	ϕ (fraction)	0.005
Microfracture tortuosity	τ (dimensionless)	1.2
Microfracture aperture	h (m)	5.0 E−06
Microfracture width	w (m)	5.0 E−06/ 1.0 E−05/ 2.0 E−05
Initial pressure	p_{int} (Pa)	1.7 E+07
Final pressure	p_{final} (Pa)	1.02
temperature	T (K)	423
Gas molar mass	M (kg/mol)	1.60 E−02
Gas viscosity	μ (Pa·s)	1.75 E−05
Universal gas constant	R (J/mol/K)	8.3144621
Mole volume of gas at standard temperature and pressure state	V_{std} (m^3/mol)	0.022414
Gas slip constant	b (dimensionless)	−1
Rarefaction coefficient	α (dimensionless)	in Figure 5

flux will continually increase; however, even if the Knudsen number is very high, Eq. 7 cannot be degraded to a Knudsen diffusion equation and cannot describe the gas Knudsen diffusion.

Knudsen diffusion

When the Knudsen number $Kn \geq 1$, the wall-molecule collisions dominate and the flow mechanism is Knudsen diffusion, the gas diffusion flux in a circular tube with a radius of h can be expressed with the Knudsen equation[5,64]

$$J_k = -\frac{\phi}{\tau} h^3 \left(\frac{M}{2\pi RT}\right)^{0.5} \frac{dp}{dl} \tag{8}$$

where J_k is the gas Knudsen diffusion flux, kg/s.

Considering the influence of section shape, the gas Knudsen flux in a microfracture with a rectangular section can be expressed as[19]

$$J_k = -B(\zeta) \frac{\phi}{\tau} h^3 \left(\frac{M}{2\pi RT}\right)^{0.5} \frac{dp}{dl} \tag{9}$$

where

$$B(\zeta) = \left\{ \zeta^2 \ln\left[\frac{1}{\zeta} + \sqrt{1+\frac{1}{\zeta^2}}\right] + \zeta \ln\left[\zeta + \sqrt{1+\zeta^2}\right] - \frac{(\zeta^2+1)^{3/2}}{3} + \frac{(1+\zeta^3)}{3} \right\} \tag{10}$$

$B(\zeta)$ is the section shape factor of the microfracture for Knudsen diffusion, dimensionless, which is not influenced by the variation of Kn, as shown in Figure 4. Compared with the gas slip flow flux, the Knudsen diffusion flux is independent of gas viscosity and gas pressure.[65]

Model establishment

In order to reasonably characterize the contributions of different transport mechanisms to gas transport in microfractures of shale and tight sandstone reservoirs, the gas transport model in microfractures is proposed by coupling the slip flow and Knudsen diffusion with the weighted coefficients relating to the ratios of intermolecular collision frequency and wall-molecule collision frequency to the total collision frequency.

The intermolecular collision frequency in microfractures can be calculated as[19,28]

$$f_m = \frac{v}{\lambda} nhwdl \tag{11}$$

where f_m is the intermolecular collision frequency, 1/s; v is the average gas thermal kinematic velocity, m/s; n is the number of gas molecules per unit volume, $1/m^3$.

The wall-molecule collision frequency in microfractures can be expressed as[19,28]

$$f_w = \frac{1}{4} nv2(h+w)dl \tag{12}$$

where f_w is the wall-molecule collision frequency, 1/s.

The weighted coefficient for slip flow is the ratio of the intermolecular collision frequency to the total collision frequency

$$\omega_{vs} = \frac{f_m}{f_m + f_w} = \frac{1}{1 + \frac{K_n\left(1+\frac{1}{\zeta}\right)}{2}} \tag{13}$$

where ω_{vs} is the ratio of the intermolecular collision frequency to the total collision frequency, fraction.

The weighted coefficient for Knudsen diffusion is the ratio of the wall-molecule collision frequency to the total collision frequency

$$\omega_k = \frac{f_w}{f_m + f_w} = \frac{1}{1 + \frac{2}{K_n\left(1+\frac{1}{\zeta}\right)}} \tag{14}$$

where ω_k is the ratio of the wall-molecule collision frequency to the total collision frequency, fraction.

Combining Eqs. 7, 9, 13, and 14, the gas transport model in microfractures can be expressed as

$$J_t = \omega_{vs} J_{vs} + \omega_k J_k \tag{15}$$

where J_t is the gas transport mass flux in microfractures, kg/s.

Model Validation

In order to check the model reliability, the calculated results are compared with the published molecular simulation results. Based on the continuum flow and Knudsen diffusion fluxes, the dimensionless gas transport flux in microfractures can be expressed as

$$\frac{J_t}{J_v} = \omega_{vs} A(\zeta)(1+\alpha Kn)\left(1 + \frac{6Kn}{1-bKn}\right) + \omega_k \frac{12Kn}{\pi} \frac{B(\zeta)}{\zeta} \tag{16}$$

$$\frac{J_t}{J_k} = \omega_{vs} \frac{\pi}{12Kn} \zeta A(\zeta)(1+\alpha Kn)\left(1 + \frac{6Kn}{1-bKn}\right) + \omega_k B(\zeta) \tag{17}$$

where J_t/J_v is the dimensionless gas transport flux based on continuum flow, dimensionless; J_t/J_k is the dimensionless gas transport flux based on Knudsen diffusion, dimensionless.

The model parameters are summarized in Table 3 and the corresponding results are shown in Figure 6.

Figure 6 shows that (1) in the microfractures with different section shapes, when $10^{-2} < Kn < 10$, the dimensionless gas flux by Scott and Dullien model only for circular section and Javadpour model with a contribution weight of 1, both have great discrepancy, compared with molecular simulation data published by Sone and Hasegawa.[66] Furthermore, the results for Javadpour model overestimate the gas transport flux; (2) the dimensionless gas flux by new model has great consistency with molecular simulation data, indicating that the model can

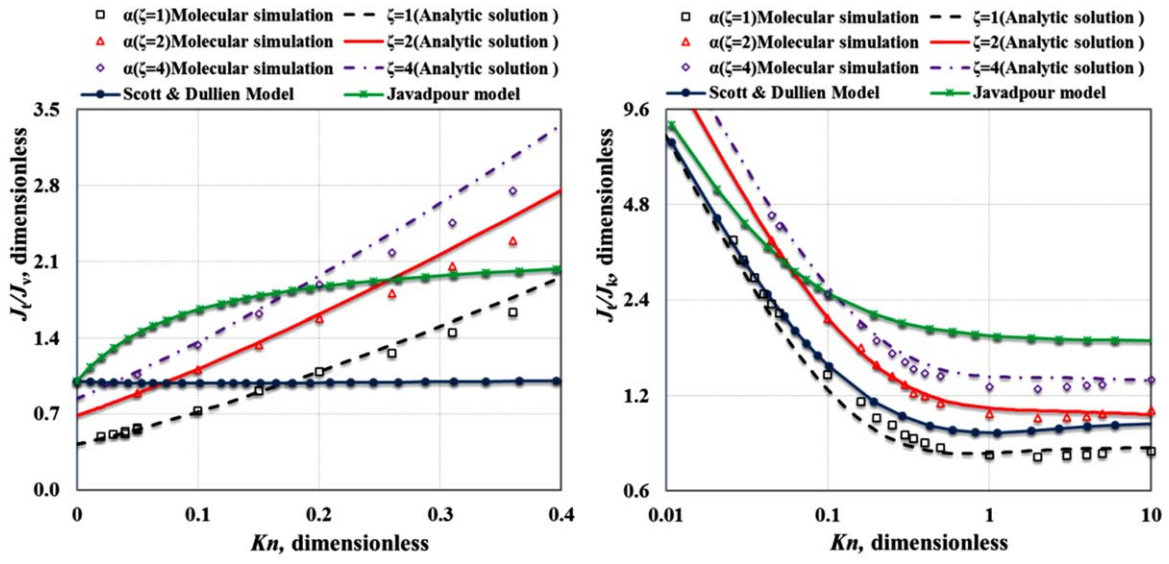

(a) $J_t/J_v \sim Kn$ (b) $J_t/J_k \sim Kn$

Figure 6. Comparison of analytic solution calculated by the new model and other data.

Note: the molecular simulation data are obtained by a linear lattice Boltzmann method.[66] [Color figure can be viewed in the online issue, which is available at wileyonlinelibrary.com.]

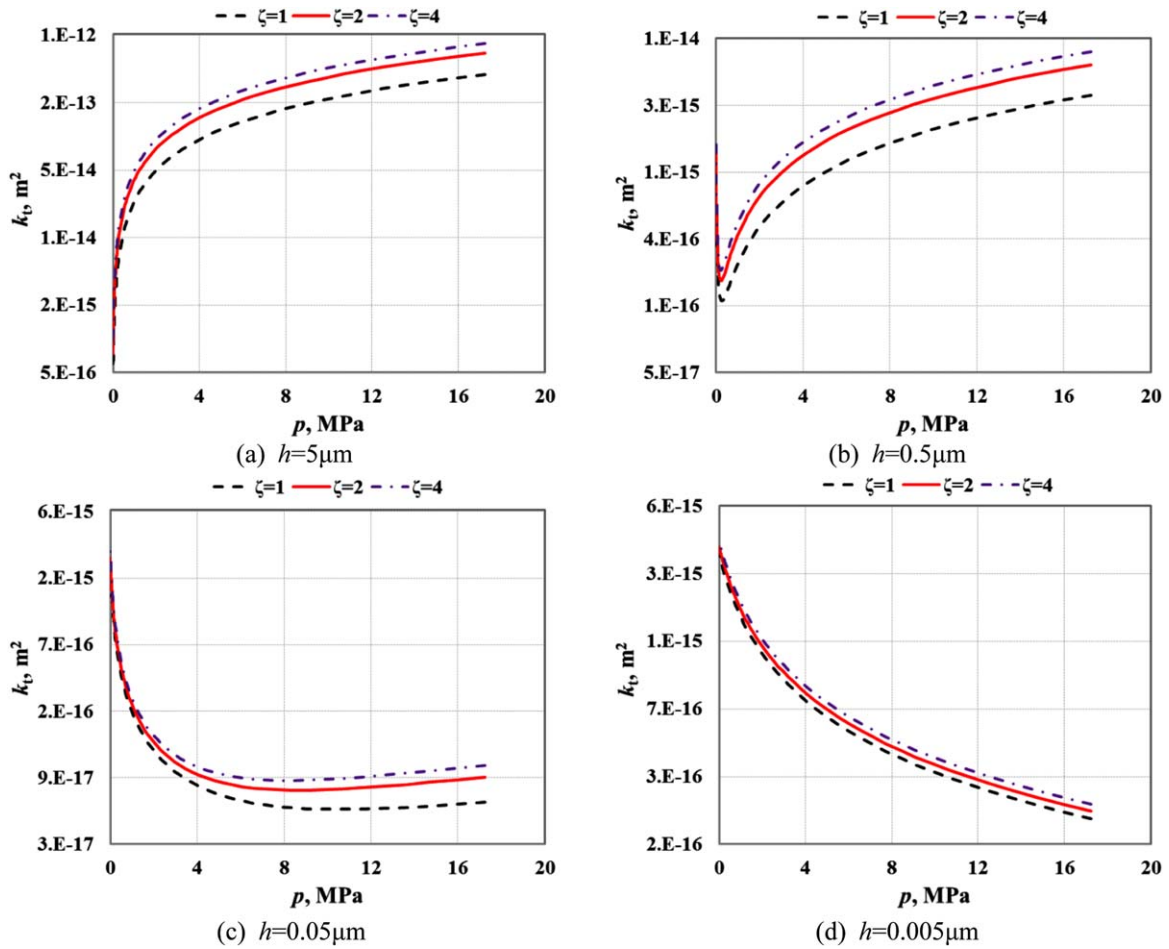

(a) h=5μm (b) h=0.5μm

(c) h=0.05μm (d) h=0.005μm

Figure 7. The curves for $k_t \sim p$ with different apertures and aspect ratios of microfractures.

(a) $h = 5$ μm, (b) $h = 0.5$ μm, (c) $h = 0.05$ μm, and (d) $h = 0.005$ μm. [Color figure can be viewed in the online issue, which is available at wileyonlinelibrary.com.]

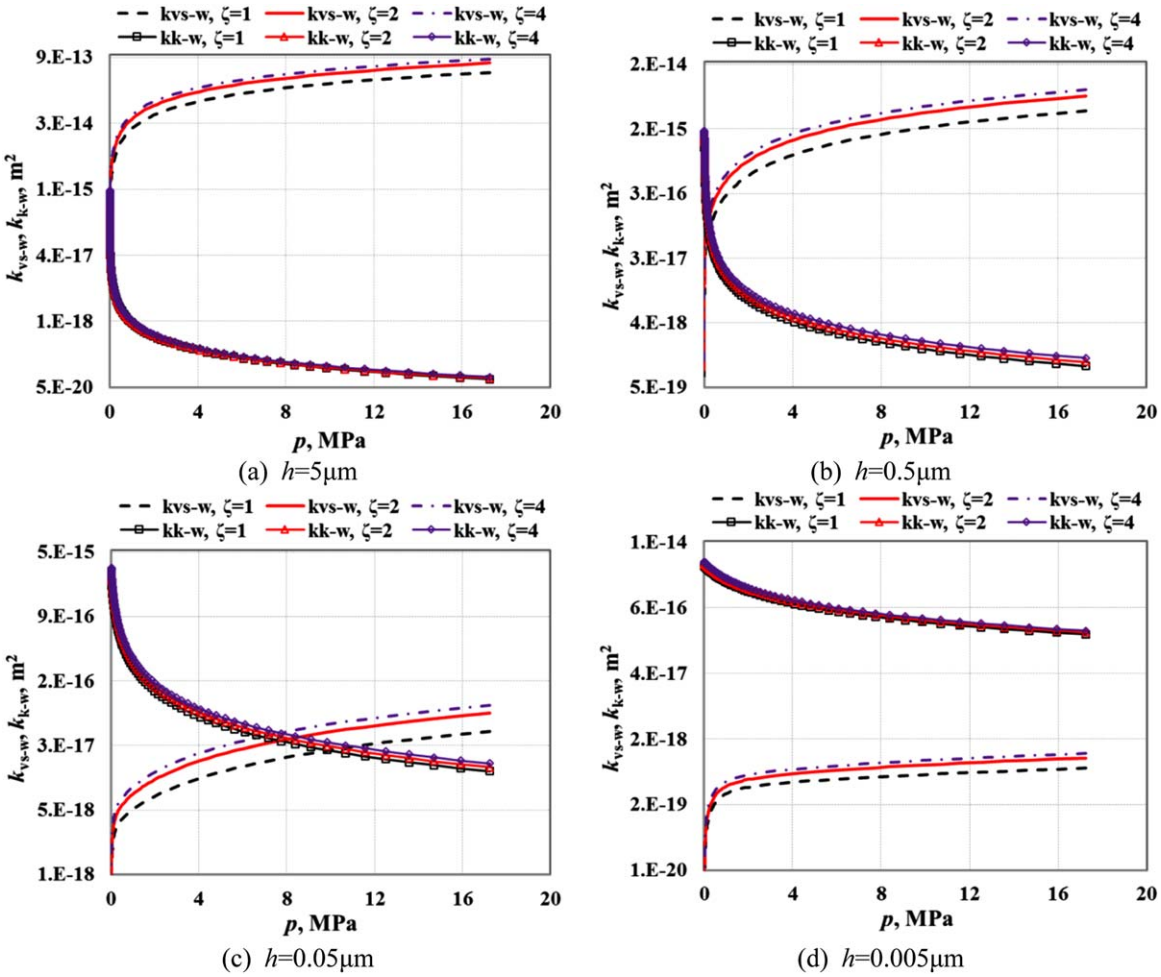

Figure 8. The curves for $k_{vs\text{-}w}$ and $k_{k\text{-}w} \sim p$ with different apertures and aspect ratios of microfractures.

(a) $h = 5$ μm, (b) $h = 0.5$ μm, (c) $h = 0.05$ μm, and (d) $h = 0.005$ μm. [Color figure can be viewed in the online issue, which is available at wileyonlinelibrary.com.]

describe the gas transport process with the coexistence of several transport mechanisms; (3) in the range of all Knudsen numbers, the minimum gas flux and dimensionless gas flux appear when $Kn = 1$, which is consistent with the gas flux obtained by molecular simulation or experiments.[16,37,67–69] It also indicates that, during the gas transport process in microfractures, the gas flux decreases and then increases with an increase in the Knudsen number, which is consistent with the practical phenomenon that gas flux decreases slowly in the later time of production in shale reservoirs.[70–73]

Results and Discussion

The gas transport in microfractures is influenced by the section shape and size, and the contributions of slip flow and Knudsen diffusion on gas transport change gradually under different depressurization production periods. For convenience, the contribution of each transport mechanism on gas transport can be expressed in the form of apparent permeability

$$k_{vs-w} = -\omega_{vs}\frac{\mu V_{std}}{Mwh}\frac{J_{vs}}{dp/dl} = \omega_{vs}A(\zeta)\frac{\phi h^2 p V_{std}}{\tau 12\ RT}(1+\alpha Kn)\left(1+\frac{6Kn}{1-bKn}\right) \tag{18}$$

$$k_{k-w} = -\omega_k\frac{\mu V_{std}}{Mwh}\frac{J_k}{dp/dl} = \omega_k B(\zeta)\frac{\phi}{\tau}\frac{h^2}{w}\mu V_{std}\left(\frac{1}{2\pi MRT}\right)^{0.5} \tag{19}$$

$$k_t = -\frac{\mu V_{std}}{Mwh}\frac{J_t}{dp/dl} = k_{vs-w} + k_{k-w} \tag{20}$$

where $k_{vs\text{-}w}$ is the apparent permeability of gas slip flow in microfractures, m^2; V_{std} is the gas mole volume at the standard state, 22.414 $\times 10^{-3}$ m^3/mol; $k_{k\text{-}w}$ is the apparent permeability of gas Knudsen diffusion in microfractures, m^2; k_t is the apparent permeability of gas transport in microfractures, m^2.

According to Eqs. 18–20, the calculation results are shown in Figures 7–9.

As shown in Figures 7a, b, when the microfracture aperture $h \geq 0.5$ μm, the gas transport capacity decreases with the decreasing pressure and microfracture aperture due to the dominance of gas slip flow in microfractures. As can be seen in Figure 7c, when the microfracture aperture $h = 0.05$ μm, the gas transport capacity first decreases and then increases with a decrease in pressure. This is because the gas slip flow dominates first and then

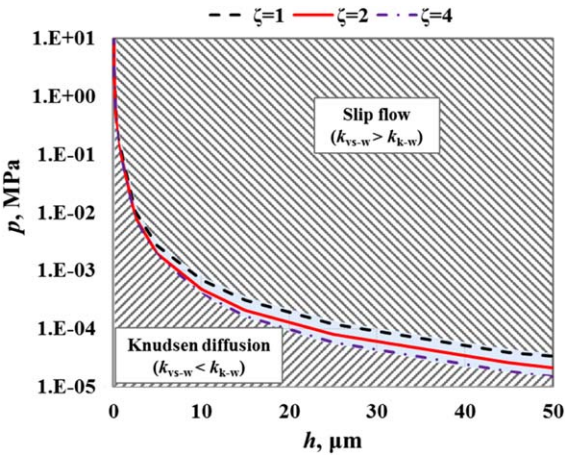

Figure 9. Cross plot of $p \sim h$ with different aspect ratios of microfractures in shale and tight gas reservoirs.

[Color figure can be viewed in the online issue, which is available at wileyonlinelibrary.com.]

Knudsen diffusion; at the same time, the gas rarefaction and slippage effects strengthen gradually. As can be seen in Figure 7d, when the microfracture aperture $h = 0.005$ μm, the gas transport capacity continually increases with the decreasing pressure. This is due to the dominance of Knudsen diffusion and the obvious rarefaction and slippage effects. It can be indicated by Figures 7a–d that, under the same aperture in microfractures, the higher the aspect ratio is, the stronger the gas transport capacity is, which is more pronounced under high gas pressure and large microfracture aperture.

According to Figures 8a–d, the apparent permeability of gas slip flow in microfractures decreases with a decrease in pressure and the apparent permeability of Knudsen diffusion increases with a decrease in pressure; both apparent permeabilities increase with an increase in the aspect ratio. Figures 8a, b show that when the microfracture aperture $h \geq 0.5$ μm, slip flow dominates in microfractures and Knudsen diffusion could be ignored. Figure 8c indicates that when the microfracture aperture $h = 0.05$ μm, slip flow and Knudsen diffusion have a similar contribution to the gas transport in microfractures. Figure 8d demonstrates that when the microfracture aperture $h \leq 0.005$ μm, Knudsen diffusion dominates in microfractures and slip flow could be ignored.

Figure 9 shows the cross plot of gas pressure and microfracture aperture, and the curve is a contour of the apparent permeability for slip flow and Knudsen diffusion. The slip flow dominates in the upper right region and the Knudsen diffusion dominates in the lower left region. The slip flow dominates the region with higher microfracture aperture and pressure, and the Knudsen diffusion dominates the region with lower microfracture aperture and pressure. The apparent permeability contour curve moves to the lower left region with an increase in the microfracture aspect ratio. The reason is that lower pressure is required for the microfracture with a high aspect ratio in order to achieve equal contribution of slip flow and Knudsen diffusion, compared with that with a low aspect ratio under the same microfracture aperture.

Conclusions

A model for gas transport in microfractures of shale and tight gas reservoirs is proposed, which can describe all the gas transport mechanisms including continuum flow, slip flow, and Knudsen diffusion.

This model can describe the variable contribution of each mechanism on the gas transport in microfractures during different production stages.

The results indicate that the gas transport capacity is influenced by section shape and sizes of microfractures. Under the same aperture, the higher the aspect ratio is, the stronger the gas transport capacity is; this phenomenon is more pronounced under the condition of higher gas pressure and larger microfracture aperture.

This article does not discuss the effects of stress dependence of permeability and real gas on the gas transport in shale and tight gas reservoirs, which will be investigated in our future paper.

Acknowledgments

The National Science and Technology Major Project of China (2011ZX05030-005-04) and National Natural Science Foundation of China (51374222 and 51490654) supported part of this work. Support of NSERC/AIEES/Foundation CMG and AITF Chairs is also acknowledged.

Literature Cited

1. Chen J, Xiao XM. Evolution of nanoporosity in organic-rich shales during thermal maturation. *Fuel*. 2014;129:173–181.
2. Rahmanian M, Solano N, Aguilera R. Storage and Output Flow from Shale and Tight Gas Reservoirs. SPE Western Regional Meeting, Anaheim, California, 2010.
3. Solano NA. Reservoir Characterization of the Upper Jurassic—Lower Cretaceous Nikanassin Group. MSc thesis, Canada: University of Calgary, Calgary, 2010.
4. Chalmers GR, Bustin RM, Power IM. Characterization of gas shale pore systems by porosimetry, pycnometry, surface area, and field emission scanning electron microscopy/transmission electron microscopy image analyses: examples from the Barnett, Woodford, Haynesville, Marcellus, and Doig units. *AAPG Bull*. 2012;96(6):1099–1119.
5. Singh H, Javadpour F, Ettehadtavakkol A, Darabi H. Nonempirical apparent permeability of shale. *SPE Reservoir Eval Eng*. 2014;17(3):414–424.
6. Aguilera R. Role of Natural Fractures and Slot Porosity on Tight Gas Sands. SPE Unconventional Reservoirs Conference, Keystone, Colorado, 2008.
7. Mohammad R, Aguilera R, Kantzas A. A new unified diffusion—viscous-flow model based on pore-level studies of tight gas formations. *SPE J*. 2012;18(1):38–49.
8. Veltzke T, Thöming J. An analytically predictive model for moderately rarefied gas flow. *J Fluid Mech*. 2012;698:406–422.
9. Bai BJ, Elgmati M, Zhang H, Wei M. Rock characterization of Fayetteville shale gas plays. *Fuel*. 2013;105:645–652.
10. Gale JFW, Reed RM, Holder J. Natural fractures in the Barnett shale and their importance for hydraulic fracture treatments. *AAPG Bull*. 2007;91(4):603–622.
11. Slatt RM, O'brien NR. Pore types in the Barnett and Woodford gas shales: contribution to understanding gas storage and migration pathways in finegrained rocks. *AAPG Bull*. 2011;95(12):2017–2030.
12. Shabro V, Torres-verdín C, Sepehrnoori K. Forecasting Gas Production in Organic Shale with the Combined Numerical Simulation of Gas Diffusion in Kerogen, Langmuir Desorption from Kerogen Surfaces, and Advection in Nanopores. SPE Annual Technical Conference and Exhibition, San Antonio, Texas, 2012.
13. Shabro V, Torres-verdín C, Javadpour F. Numerical Simulation of Shale-Gas Production: From Pore-Scale Modeling of Slip-Flow,

Knudsen Diffusion, and Langmuir Desorption to Reservoir Modeling of Compressible Fluid. Unconventional Gas Conference, the Woodlands, Texas, 2011.
14. Wu KL, Li XF, Wang CC, Yu W, Guo CH, Ji DQ, Ren GX, Chen ZX. Apparent Permeability for Gas Flow in Shale Reservoirs Coupling Effects of Gas Diffusion and Desorption. Unconventional Resources Technology Conference, Denver, Colorado, 2014.
15. Browne VA, John JEA. Vacuum radial flow from the viscous through the free molecule regime. *Vacuum*. 1970;20(12):525–533.
16. Sun YH, Chan WK. Analytical modeling of rarefied Poiseuille flow in microchannels. *J Vac Sci Technol A*. 2004;22(2):383–394.
17. Deng J, Zhu WY, Ma Q. A new seepage model for shale gas reservoir and productivity analysis of fractured well. *Fuel*. 2014;124:232–240.
18. Ma JS, Sanchez JP, Wu KJ, Couples GD, Jiang ZY. A pore network model for simulating non-ideal gas flow in micro- and nano-porous materials. *Fuel*. 2014;116:498–508.
19. Thompson SL, Owens WR. A survey of flow at low pressures. *Vacuum*. 1975;25(4):151–156.
20. Okabe H. Pore-Scale Modeling of Carbonates. PhD dissertation, London, UK: Imperial College, 2004.
21. Okabe H, Blunt MJ. Pore space reconstruction using multiple-point statistics. *J Petrol Sci Eng*. 2005;46(1–2):121–137.
22. Hooker JN, Gale JFW, Gomez LA, Laubach SE, Marrett R, Reed RM. Aperture size scaling variations in a low-strain opening-mode fracture set, Cozzette Sandstone, Colorado. *Struct Geol*. 2009;31(7):707–718.
23. Aguilera RF, Ramirez JF, Ortega CE. A Variable Shape Distribution (VSD) Model for Characterization of Pore Throat Apertures, Petrophysical Properties and Drill Cuttings in Conventional, Tight and Shale Reservoirs. SPE Asia Pacific Oil and Gas Conference and Exhibition, Perth, Australia, 2012.
24. Soeder DJ, Randolph PJ. Porosity, permeability, and pore structure of the tight Mesaverde sandstone, Piceance Basin, Colorado. *SPE Form Eval*. 1987;2(2):129–136.
25. Soeder DJ, Chowdiah P. Pore geometry in high-and low-permeability sandstones, Travis Peak Formation, East Texas. *SPE Form Eval*. 1990;5(4):421–430.
26. Shanley KW, Cluff RM, Robinson JW. Factors controlling prolific gas production from low-permeability sandstone reservoirs: implications for resource assessment, prospect development, and risk analysis. *AAPG Bull*. 2004;88(8):1083–1121.
27. Sun YP, Wu QH, Wei MZ, Bai BJ, Ma YF. Experimental study of friction reducer flows in microfracture. *Fuel*. 2014;131:28–35.
28. Karniadakis G, Beskok A, Aluru NR. *Microflows and Nanoflows: Fundamentals and Simulation*. New York: Springer Verlag, 2005.
29. Smolouchowski M. *Transpiration und Diffusion Verdunnter Gase*. *Ann Phys*. 1910;33:1559–1570.
30. Kennard EH. *Kinetic Theory of Gases*. New York: McGraw-Hill, 1938.
31. Eldridge BD, Brown LF. The effect of cross sectional pore shape on Knudsen diffusion in porous materials. *AIChE J*. 1976;22(5):942–944.
32. Matson SL, Quinn JA. Knudsen diffusion through noncircular pores: textbook errors. *AIChE J*. 1977;23(5):768–770.
33. White FM. *Viscous Fluid Flow*, *2nd ed*. New York: McGraw-Hill, 1991.
34. Wu YS, Pruess K, Persoff PJ. Gas flow in porous media with Klinkenberg effects. *J Porous Media*. 1998;32 (1):117–137.
35. Piekos ES, Breuer KS. Numerical modeling of micromechanical devices using the Direct Simulation Monte Carlo Method. *J Fluids Eng*. 1996;118(3):464–469.
36. Binder K, Horbach J, Kob W, Paul W, Varni F. Molecular dynamics simulations. *J Phys: Condens Matter*. 2004;16(5):S429.
37. Loyalka S, Hamoodi S. Poiseuille flow of a rarefied gas in a cylindrical tube: solution of linearized Boltzmann equation. *Phys Fluids A*. 1990;2(11):2061–2065.
38. Gad-el-hak M. The fluid mechanics of microdevices—the freeman scholar lecture. *J Fluids Eng*. 1999;121(1):5–33.
39. Malek K, Coppens MO. Pore roughness effects on self- and transport diffusion in nanoporous materials. *Colloids Surf A: Physicochem Eng Asp*. 2002;206(1–3):335–348.
40. Koplik J, Banavar JR. Continuum deductions from molecular hydrodynamics. *Annu Rev Fluid Mech*. 1995;27:257–292.
41. Mao ZG, Sinnott SB. Separation of organic molecular mixtures in carbon nanotubes and bundles: molecular dynamics simulations. *J Phys Chem B*. 2001;105(29):6916–6924.
42. Nie XB, Chen SY, WN E, Robbins MO. A continuum and molecular dynamics hybrid method for micro- and nano-fluid flow. *J Fluid Mech*. 2004;500:55–64.
43. Coppens MO, Dammers AJ. Effects of heterogeneity on diffusion in nanopores from inorganic materials to protein crystals and ion channels. *Fluid Phase Equilib*. 2006;246(1–2):308–316.
44. Roy S, Raju R, Chuang HF, Cruden BA, Meyyappan M. Modelling gas flow through microchannels and nanopores. *J Appl Phys*. 2003;93(8):4870–4879.
45. Javadpour F, Fisher D, Unsworth M. Nanoscale gas flow in shale gas sediments. *J Can Petrol Technol*. 2007;46(10):55–61.
46. Javadpour F. Nanopores and apparent permeability of gas flow in mudrocks (shales and siltstone). *J Can Petrol Technol*. 2009;48(8):16–21.
47. Civan F, Devegowda D, Sigal R. Critical evaluation and improvement of methods for determination of matrix permeability of shale. SPE Annual Technical Conference and Exhibition, New Orleans, Louisiana, 2013.
48. Civan F. Effective correlation of apparent gas permeability in low-permeability porous media. *Transp Porous Media*. 2010;82(2):375–384.
49. Civan F, Rai CS, Sondergeld CH. Shale-gas permeability and diffusivity inferred by improved formulation of relevant retention and transport mechanisms. *Transp Porous Media*. 2011;86(3):925–944.
50. Prince A, Javadpour F. Dual-continuum modeling of shale and tight gas reservoirs. SPE Annual Technical Conference and Exhibition, San Antonio, Texas, 2012.
51. Darabi H, Ettehad A, Javadpour F, Sepehrnoori K. Gas flow in ultra-tight shale strata. *J Fluid Mech*. 2012;710:641–658.
52. Shen S, Chen G, Cronel RM, Anaya-Dufresne M. A kinetic-theory based first order slip boundary condition for gas flow. *Phys Fluids*. 2007;19(8):086101.
53. Maurer J, Tabeling P, Joseph P, Willaime H. Second-order slip laws in microchannels for helium and nitrogen. *Phys Fluids*. 2003;15(9):2613.
54. Beskok A, Karniadakis GE. A model for flows in channels, pipes, and ducts at micro and nano scales. *Microscale Thermophys Eng*. 1999;3(1):43–77.
55. Adzumi H. Studies on the flow of gaseous mixtures through capillaries. *I. the viscosity of binary gaseous mixtures*. *Bull Chem Soc Jpn*. 1937;12(5):199–226.
56. Adzumi H. Studies on the flow of gaseous mixtures through capillaries. *II. The molecular flow of gaseous mixtures*. *Bull Chem Soc Jpn*. 1937;12(6):285–291.
57. Adzumi H. Studies on the flow of gaseous mixtures through capillaries. *III. The flow of gaseous mixtures at medium pressures*. *Bull Chem Soc Jpn*. 1937;12(6):292–303.
58. Brown GP, Dinardo A, Cheng GK, Sherwood TK. The flow of gases in pipes at low pressures. *J Appl Phys*. 1946;17(10):802.
59. Scott DS, Dullien FAL. Diffusion of ideal gases in capillaries and porous solids. *AIChE J*. 1962;8(1):113–117.
60. Ertekin T, King G,Schwerer F. Dynamic gas slippage: a unique dual-mechanism approach to the flow of gas in tight formations. *SPE Form Eval*. 1986;1(1):43–52.
61. Chen ZX, Ewing RE. *Fluid Flow and Transport in Porous Media: Mathematical and Numerical Treatment*. Massachusetts: American Mathematical Society, 2001.
62. Li ZP, Li ZF. Dynamic seepage characteristics of shale gas nanoscale pores. *Nat Gas Ind*. 2012;32(4):1–4. (in Chinese).
63. Loeb LB. *The Kinetic Theory of Gases*, 2nd ed. New York: McGraw-Hill, 1934.
64. Peters EJ. *Advanced Petrophysics: Vol. 2: Dispersion, Interfacial Phenomena/Wettability, Capillarity/Capillary Pressure, Relative Permeability*. Greenleaf Book Group, Austin, Texas, US. 2012.
65. Choi JG, Do DD, Do HD. Surface diffusion of adsorbed molecules in porous media: monolayer, multilayer, and capillary condensation regimes. *Ind Eng Chem Res*. 2001;40(19):4005–4031.
66. Sone Y, Hasegawa M. Poiseuille and thermal transpiration flows of a rarefied gas through a rectangular pipe. *J Vac Soc Jpn*. 1987;30:425–428. (in Japanese).
67. Cercignani C. *Theory and Applications of the Holzmann Equation*. New York: Elsevier, 1975.

68. Williams MMR. *Mathematical Methods in Particle Transport Theory*. London: Butterworths, 1971.
69. Kogan MN. *Rarefied Gas Dynamics*. New York: Plenum, 1969.
70. Zhang LH, Chen G, Zhao YL, Liu QF, Zhang HC. A modified material balance equation for shale gas reservoirs and a calculation method of shale gas reserves. *Nat Gas Ind*. 2013;33(12):66–70. (in Chinese).
71. Yu RZ, Zhang XW, Bian YN, Li Y, Hao MX. Flow mechanism of shale gas reservoirs and influential factors of their productivity. *Nat Gas Ind*. 2012;32(9):10–15. (in Chinese).
72. Zhang XT, Wu JF, Feng X, Deng H, Yang JY. Numerical simulation of seepage flow characteristics of multi-stage fracturing (MSF) in horizontal shale gas wells. *Nat Gas Ind*. 2013;33(3):47–52. (in Chinese).
73. Wua KL, Li XF, Guo CH, Chen ZX. Adsorbed gas surface diffusion and bulk gas transport in nanopores of shale reservoirs with real gas effect-adsorption-mechanical coupling. *SPE Reservoir Simulation Symposium*, Houston, Texas, 2015.

Manuscript received Sep. 15, 2014, and revision received Mar. 4, 2015.